Controls on buffering and coastal acidification in a temperate estuary

Christopher W. Hunt ,* Joseph E. Salisbury , Douglas Vandemark
Ocean Process Analysis Laboratory, University of New Hampshire, Durham, New Hampshire

Abstract

Estuaries may be uniquely susceptible to the combined acidification pressures of atmospherically driven ocean acidification (OA), biologically driven CO_2 inputs from the estuary itself, and terrestrially derived freshwater inputs. This study utilized continuous measurements of total alkalinity (TA) and the partial pressure of carbon dioxide (pCO_2) from the mouth of Great Bay, a temperate northeastern U.S. estuary, to examine the potential influences of endmember mixing and biogeochemical transformation upon estuary buffering capacity (β–H). Observations were collected hourly over 28 months representing all seasons between May 2016 and December 2019. Results indicated that endmember mixing explained most of the observed variability in TA and dissolved inorganic carbon (DIC), concentrations of which varied strongly with season. For much of the year, mixing dictated the relative proportions of salinity-normalized TA and DIC as well, but a fall season shift in these proportions indicated that aerobic respiration was observed, which would decrease β–H by decreasing TA and increasing DIC. However, fall was also the season of weakest statistical correspondence between salinity and both TA and DIC, as well as the overall highest salinity, TA and β–H. Potential biogeochemically driven β–H decreases were overshadowed by increased buffering capacity supplied by coastal ocean water. A simple modeling exercise showed that mixing processes controlled most monthly changes in TA and DIC, obscuring impacts from air–sea exchange or metabolic processes. Advective mixing contributions may be as important as biogeochemically driven changes to observe when evaluating local estuarine and coastal OA.

Balanced at the confluence of the land and sea, estuaries are dynamic mixing zones, sites of biogeochemical transformations and enrichments, and essential habitats in the life cycles of many species. The continuous, complex journey of dissolved and particulate materials derived from terrestrial sources through an estuary proceeds along a number of dimensions in space and time (Gattuso et al. 1998; Borges 2005). Along one dimension, substances are carried by rivers and groundwater into the estuary, where they are physically mixed with coastal seawater while utilized and altered by pelagic and benthic organisms. Vertical exchanges between the pelagic water column, benthic sediments and the

atmosphere add a vertical dimension of complexity (Cai et al. 2017), while mixing of water and associated materials within certain ecosystems such as mangroves and salt marshes provide another lateral dimension (Wang and Cai 2004; Sippo et al. 2016; Wang et al. 2016). Finally, all of the above mechanisms may be altered over time by shifts in temperature and salinity, changes in freshwater discharge and associated changes in constituent loads, seasonal and episodic alterations in net ecosystem productivity, anthropogenic watershed and ecosystem modifications, variations in coastal ocean exchange, and other short- and long-term factors (Waldbusser and Salisbury 2014; Lee et al. 2015; Pacella et al. 2018).

Against this backdrop of complex biogeochemical changes, estuaries are also situated as hotspots of acidification (Cai et al. 2020). The accumulation of anthropogenic carbon dioxide (CO_2) in the atmosphere has led to a compensatory increased uptake of CO_2 by the global ocean in a process termed ocean acidification (OA; Orr et al. 2005, Doney et al. 2009), which has driven down seawater pH by about 0.1 units since the start of the Industrial Revolution and threatens to further lower pH by another 0.3 by the end of the 21st century (IPCC 2021). In addition to OA, estuaries are also under acidification pressure from coastal-specific processes grouped into the term coastal acidification (CA). CA refers to factors such as nutrient-enhanced productivity and the

Additional Supporting Information may be found in the online version of this article.

biochemical pathway of the subsequent decomposition of the produced organic material (Breitburg et al. 2015), shifts in the amount and composition of freshwater discharge (Salisbury et al. 2008; Kaushal et al. 2013, 2014), submarine groundwater discharge (Wang et al. 2014), and atmospheric acid deposition (Doney et al. 2007; Duarte 2013). The combined effects of OA and CA are termed ocean and coastal acidification (OCA), which result in changes in pH and other properties due to both local and remote forcing (Gledhill et al. 2015). The capacity of a water body to resist changes in acid level is termed buffering and can be parameterized using the concentrations of total alkalinity (TA) and dissolved inorganic carbon (DIC) in that water body (Egleston et al. 2010, Middelburg et al. 2020). Changes to both the absolute concentrations and the relative proportions of TA and DIC can have potentially profound effects on the buffering capacity (and consequently pH) of an estuary; thus the influences of mixing and biogeochemical transformations of TA and DIC in an estuary are important to understand in light of growing OCA pressures.

Estuaries are generally thought to enrich DIC through the respiration of allochthonous and autochthonous organic carbon and transport of river and coastal wetland DIC (Borges et al. 2003; Bauer et al. 2013; Sippo et al. 2016). Conversely, primary productivity and carbonate precipitation can draw down DIC. In addition, several processes have been shown to produce TA within estuaries (Supporting Information Table S1), including primary productivity, denitrification, manganese reduction, iron reduction, and sulfate reduction (Raymond et al. 2000; Borges et al. 2003; Sippo et al. 2016). Growth of calcifying organisms, such as oysters, and the harvest or burial of their shells represents a sink of TA (Waldbusser et al. 2013), as does aerobic respiration (Borges et al. 2003). In the Chesapeake Bay, Waldbusser et al. (2013) estimated a TA sink of 2.25 mol m^2 yr^1. In the temperate York River estuary, Raymond et al. (2000) attributed additions of TA and DIC to sulfate reduction. In mangroves, TA export estimates range from 1.2 to 117 mmol m^2 d^1 (Leopold et al. 2016; Sippo et al. 2016), while mangroves may account for up to 93% of DIC exports in a watershed (Faber et al. 2014). Several studies have identified sulfate reduction and aerobic respiration as the major organic matter remineralization pathways in mangroves which control TA and DIC exports (Borges et al. 2003; Bouillon et al. 2007; Sippo et al. 2016). Salt marshes have also been described as "CO_2 Pumps"-absorbing CO_2 from the atmosphere and exporting the resulting inorganic carbon (at least partly as TA) to the coastal zone, likely via anerobic respiration or sulfate reduction (Wang and Cai 2004). Several salt marsh systems have been shown to follow this mechanism; however, these studies have been limited to sites containing a large proportion of marsh habitat (Cai and Wang 1998; Wang and Cai 2004) or were based on discrete sampling at monthly or seasonal time scales, which may not capture shorter-scale variability. Estuaries are also frequently mixed-habitat areas, with

a wide array of processes and natural and anthropogenic factors combining to affect the TA and DIC exchange with the coastal ocean. Mixing in estuaries is also complex as counteracting flows of coastal and river water produce variable patterns of vertical, horizontal and cross- channel mixing (Lerczak and Rockwell Geyer 2004). In addition, the dynamics of TA and DIC production, consumption and exchange may change episodically, seasonally, or on an interannual basis.

Estuaries and coastal waters in New England have been identified as particularly vulnerable to the effects of OCA due to atmospheric acid deposition (Driscoll et al. 2001; Doney et al. 2007), eutrophication (Rheuban et al. 2019), sedimentary processes (Fennel et al. 2008), and the convergence of rapidly warming, relatively fresh coastal ocean waters with poorly buffered rivers (Salisbury et al. 2008; Gledhill et al. 2015). Local management agencies have initiated studies of the potential effects of OCA (COMNARE 2017; MSLCOOA 2021) and called for the examination of the contributions of individual processes to overall OCA. Here, we present a study of a New England estuary using novel, highly resolved time series measurements, which can help to tease apart the processes that affect buffering, pH, and potential future OCA in this area.

Study area and methods

The Great Bay is a macrotidal estuary covering 44 km^2 in southeastern New Hampshire and southwestern Maine, USA. The Great Bay is enclosed by 230 km of generally steep rocky shoreline, bordered by narrow salt marshes, and connected to the neighboring Gulf of Maine via the Piscataqua River (Fig. 1). Great Bay contains about 9 km^2 of salt marsh, or about 20% of the total estuary area, with the remaining area comprised of clam flats, eelgrass beds, intertidal and subtidal macroalgal cover, mudflats, and rocky outcrops and islands (Jones 2000).

The University of New Hampshire's Coastal Marine Laboratory (CML) is located at the outlet of Great Bay at the mouth of the Piscataqua River. A continuously pumped intake located 0.5 m from the bottom of the Piscataqua channel supplies the CML with seawater. Water depth at this intake ranges roughly between 4 and 6 m over a typical tidal cycle (De Meo 2011). Tidal exchange and currents at this location are very strong, and previous work at this same location showed that low-tide water pumped to CML was comprised of outgoing Great Bay estuary water, while at high tide the water was near-shore western Gulf of Maine water (Brown 2006).

Sensors for the measurement of CML intake water temperature and salinity (Aanderaa 4319) and dissolved oxygen (Aanderaa 4835) were suspended in a large 200-liter open tank equipped with a passive debubbling and sediment settling system. Seawater was continuously pumped through this tank at a rate of about 5 liters per minute. Seawater was also pumped to a spray-type seawater gas equilibrator, similar to that described by Wanninkhof and Thoning (1993). Equilibrated air was drawn at 100 mL/min through tubing containing a
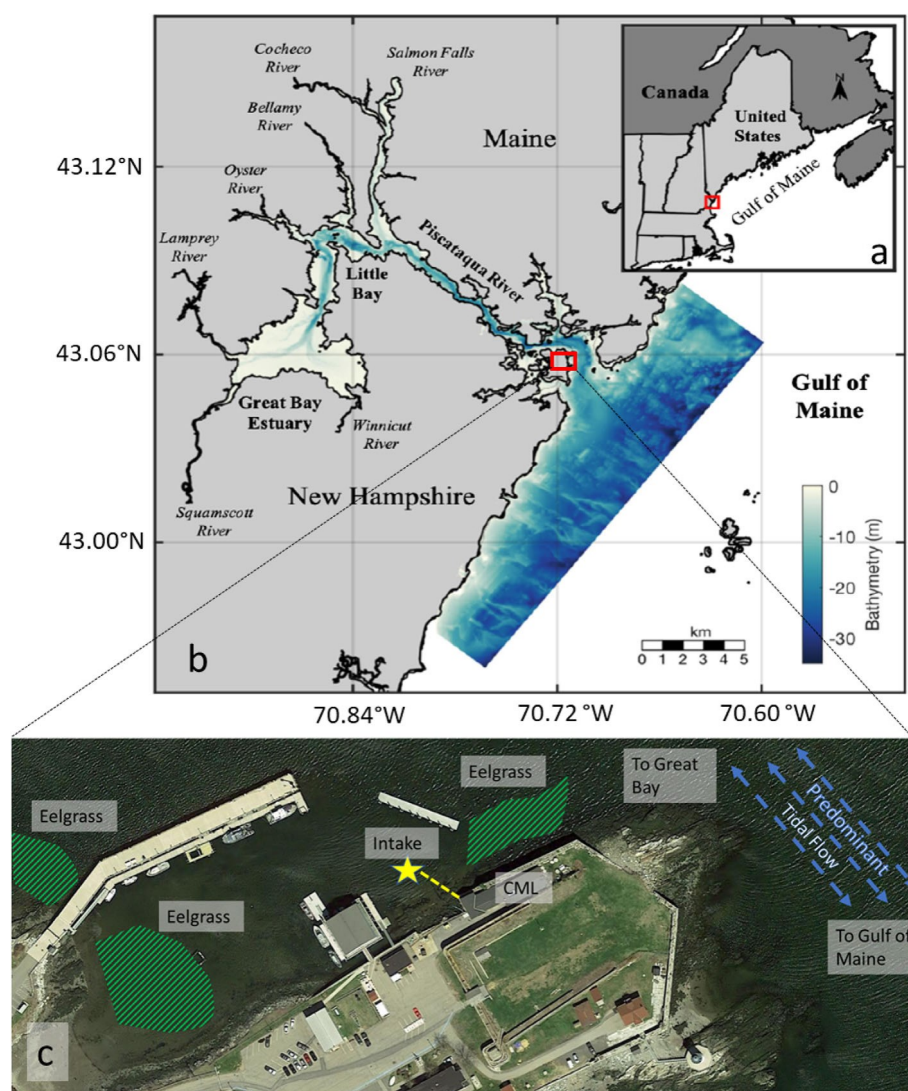
Fig. 1. The Great Bay estuary. (a) The Gulf of Maine region, with Great Bay indicated by a red box. (b) Great Bay, its bathymetry, and its contributing rivers, with the CML location shown as a red box. (c) Aerial imagery of the CML and surrounding environs, including the lab water intake (yellow), local eelgrass beds (green), and predominant tidal flow (blue). Images (a) and (b) used with permission from Cook (2019), panel (c) modified from Google Maps imagery.

Nafion selectively permeable membrane (Perma Pure), with the same analyzed sample stream at lower pressure returned through an outer tubing to carry away the stripped water vapor. This "reflux method" effectively dries the sample gas stream of water vapor with no external supply of drying gas required. No water temperature difference was observed between that measured by the Aanderaa temperature sensor in the open tank and the outflow from the equilibrator (measured with a handheld meter—YSI—manufacturer accuracy 0.2C). Temperature data from the Aanderaa sensor was used in sea-surface temperature corrections during the calculation of pCO_2. After drying, the sample was pumped to a nondispersive infrared gas analyzer (Li-cor LI-840), which measured the molar fraction of carbon dioxide (xCO_2) of the sample stream. Linearity of the Li-cor response was validated in the lab using a range of calibrated standards. The Li-cor was calibrated weekly or biweekly with pure nitrogen (0 ppm CO_2 molar fraction) and one span tank. Over the study period, we employed a succession of span tanks containing a gas mixture with CO_2 molar fraction between 500 and 850 ppm (Scott-Marin), which were calibrated against a primary standard obtained from the National Oceanic and Atmospheric Administration's Earth System Research Laboratory. Additionally, a set of switching valves operated by a computer running a custom-built software program allowed for periodic checks of pure nitrogen and span gas to monitor instrument drift. Corrections of data for water vapor pressure and sea surface temperature and conversion from xCO_2 to the partial pressure of carbon dioxide (pCO_2) were carried out according to standard methods (Dickson et al. 2007). The estimated uncertainty of pCO_2 measurements is 3 µatm.

An automated TA analyzer (Contros HydroFIA TA) was installed at CML in May 2016 and operated until November 2019, with an extended break in later 2017 when the instrument was returned for service, and a longer break from 2018 into 2019 when fire damaged the CML facility and regular operations were suspended. The HydroFIA instrument performs a single-point titration of seawater with 0.1 N hydrochloric acid, using bromocresol green as the indicator for spectrophotometric pH detection, a technique developed by Yao and Byrne (1998) and refined by Li et al. (2013). Filtered seawater (pore size 0.2 μm) was supplied to the HydroFIA instrument from a cross-flow filter supplied by Kongsberg. The HydroFIA instrument was set to perform hourly measurements, and re-calibrated on a one to 2-week interval with certified reference material (CRM) from Dr. Andrew Dickson (Dickson et al. 2003). All CML data, including measurements of TA and pCO_2, are hosted by the Northeastern Regional Coastal Ocean Observing System (http://neracoos.org).

Derived parameter calculation

The concurrent measurements of salinity, temperature, pCO_2, and TA at CML allowed for the determination of other carbonate system components. The calculation of DIC and pH (on the total scale, at a constant 25C or at in situ temperature) was performed using the CO2SYS program (van Heuven et al. 2011). The K1 and K2 constants chosen were those of Cai and Wang (1998), the KSO_4 and KB constants were those of Dickson et al. 1990 and Dickson 1990, respectively, and the total boron concentration was calculated from salinity according to Uppström (1974). Phosphate and silica concentrations were set to zero in CO2SYS, as studies have shown low nutrient concentrations in the study area (Short 1992; PREP 2017). The buffer factor β–H, was defined according to Egleston et al. (2010) as:

$$\beta_H = -\left(\frac{\partial pH}{\partial H}\right)^{-1} \tag{1}$$

β–H quantifies the change in seawater acidity due to an addition or removal of hydrogen ion. This buffer factor is related to, but not identical to, the Revelle factor which quantifies the change in the concentration of CO_2 relative to a change in DIC (Broecker et al. 1979). We chose to discuss β–H as it most directly relates to the concept of buffering acid additions or removals. A detailed description of the β–H calculation is provided in the Supporting Information.

The presence of organic constituents contributing to titration alkalinity has been shown in estuaries (Cai et al. 1998), coastal waters (Yang et al. 2015), and even reference materials (Sharp and Byrne 2021). Although organic alkalinity concentrations were shown to be generally low relative to TA, they were variable and the sources of the organic constituents were unclear. In light of these uncertainties, calculations in this study were performed under the assumption that TA did not

contain an organic component. This assumption is further discussed in the Supporting Information.

Salinity normalization approach

Some analyses in the following sections required normalization of data to a constant salinity. Various studies have used a simple technique to normalize data (e.g., normalization to a constant salinity of 35, such as described by Millero et al. 1998), but Friis et al. (2003) pointed out that this technique can lead to erroneous results if a nonzero y-intercept is present, as was the case in this study. We followed the approach of Friis et al. (2003) according to the following:

$$nTA = \frac{TA_{obs} - TA_0}{S_{obs}}S^{mean} + TA^0, \tag{2}$$

$$nDIC = \frac{DIC_{obs} - DIC_0}{S_{obs}}S^{mean} + DIC^0, \tag{3}$$

where TA_{obs} and DIC_{obs} are the observed TA and DIC, respectively, TA_0 and DIC_0 are the zero-salinity TA and DIC determined from linear regression against salinity, respectively, S_{obs} is the salinity corresponding to the observation of TA or DIC, and S_{mean} is the mean salinity of all observations used in the linear regression.

Data analysis

Linear regression analysis of salinity against TA and DIC was performed using an iteratively weighted least-squares algorithm with a bisquare weighting function and robust fitting options enabled (fitlm in Matlab®). This returned two linear coefficients: the change in TA or DIC per unit salinity (i.e., slope, designated "TA : S" or "DIC : S" hereafter) and the TA or DIC calculated at salinity zero (i.e., intercept, designated "TA_0" and "DIC_0," respectively).

Performance of the Contros HydroFIA® TA system

The HydroFIA® TA instrument collected 11,150 hourly measurements between May 2016 and November 2019. In addition, instrument checks were performed every 1–2 weeks using CRM obtained from the Scripps Institute of Oceanography laboratory of Dr. Andrew Dickson (Dickson et al. 2003) to support assessments of instrument stability and accuracy. A total of 80 sets of triplicate CRM checks were conducted over the study period, each prior to instrument recalibration (see Supporting Information Fig. S1). The magnitude of one standard deviation (σ) of the triplicate CRM checks ranged from less than 1 to 23.4 μmol kg^1, with a mean σ of 3.8 μmol kg^1. This σ is somewhat higher than that reported by Seelmann et al. (2019) for the HydroFIA® TA instrument, as well as that reported by Hunt et al. (2021) in a shipboard deployment; however, as will be shown in this work the σ from this study was adequate for resolving the dynamic TA signals at CML, both at shorter tidal and longer monthly time scales, where TA variability was greater than the mean σ by an order of magnitude or more.

The mean difference between CRM measurements and the certified TA value was 2.9 19.0 μmol kg[1], where the negative value indicates that the mean HydroFIA° TA values were lower than the CRM TA.

Deterministic model

To estimate the relative contributions of mixing, net ecosystem metabolism (NEM, Caffrey 2004), and air-sea flux of CO_2 to changes in TA and DIC, we used a deterministic model based on that of Pacella et al. (2018). Briefly, this model apportioned changes in DIC over time according to changes in mixing, NEM, and air-sea flux, while changes in TA were apportioned according to changes in mixing and NEM. The availability of hourly measurements in this study provided hourly observed values of TA and DIC and allowed for the calculation of the effects of NEM on TA and DIC (see the Supporting Information for a detailed model description).

Results

Observed conditions

Conditions at CML during the study period were strongly seasonal: colder and fresher in the winter and spring, and warmer and saltier in the summer and fall (Fig. 2, Supporting Information Table S2). The coldest monthly average water temperature was in February, while the lowest monthly average salinity was in April; the highest average water temperature was in August, while the highest average salinity was in September. Vigorous semidiurnal tidal exchanges between the coastal ocean and Great Bay produced clear temperature and salinity differences at CML between high and low tides, sometimes exceeding 5C in temperature and 5 in salinity over the tidal cycle. Salinity variability was greatest in the late winter and spring, when seasonal storms and melting snowpack brought more fresh water into Great Bay to mix with saltier coastal water. In contrast, late summer and fall typically had fewer storms and drier conditions, which resulted in much less salinity variability during these seasons. The generally dry conditions in summer and fall were reflected in low-salinity standard deviation values from July through October, while wetter spring conditions were reflected in high-salinity standard deviations from March through May (Supporting Information Table S2).

Monthly mean pCO_2 dropped through the winter to annual low values in March and April, then rose steadily to an annual high in August before dropping through the fall. In
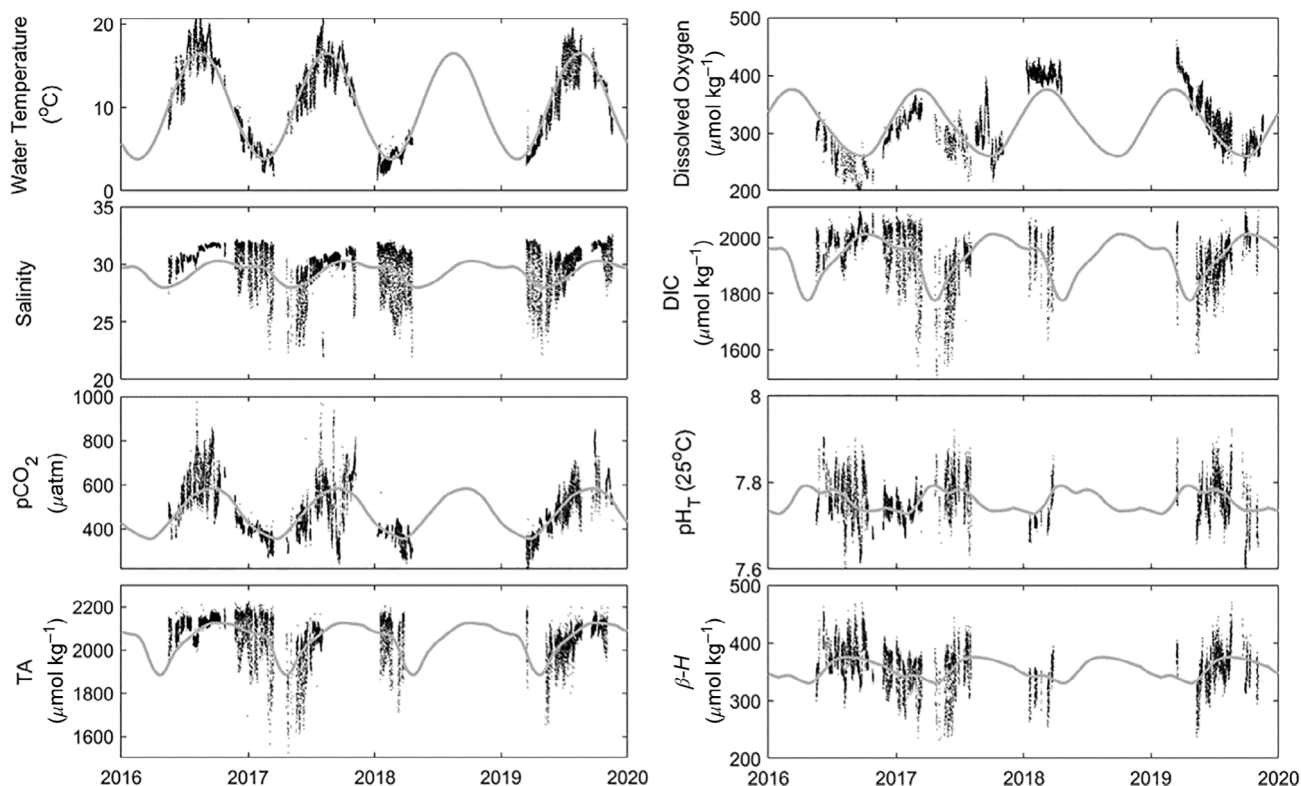

Fig. 2. Coastal Marine Laboratory hourly time series plots (black markers) measured from 2016 to 2019. Gray lines depict annual climatologies, calcu-lated from monthly averages of data from 2005 to 2019, except for TA data which were collected from 2016 through 2019. Gray lines depict annual climatologies calculated from monthly averages of data from 2016 to 2019. Refer to the text for details of the calculation of DIC, pHT, and β–H from in situ measurements of salinity, temperature, pCO_2 and TA. See Supporting Information for further detail regarding the preparation of climatologies. All monthly climatologies were smoothed over 60 d ("smooth" function, Matlab°, Mathworks).

contrast to salinity, pCO_2 variability was highest when salinity variability was lowest, as seen during the late summer and fall in 2016 (Fig. 2). This pattern was reflected in larger pCO_2 standard deviations from July to November and smaller pCO_2 standard deviations from December to May (Supporting Information Table S2). Although pCO_2 was generally higher at low tide, there were periods each year when low-tide pCO_2 was lower than high tide, typically during spring months.

TA concentrations followed the pattern of salinity, with higher TA associated with higher salinity, and higher tidal TA variability associated with periods of higher salinity variability. Monthly average TA was highest in September, which was also the month of lowest TA variability as measured by the standard deviation of monthly data (Fig. 2; Supporting Information Table S2) and highest average salinity. Although infrequent, there were periods when the TA at high tide was lower than that on the subsequent low tide, generally in summer or fall (there were no such periods of lower salinity at high tide than low tide, however). The monthly average TA was lowest in April, which was the month of lowest average salinity and highest TA variability (Supporting Information Table S2), but also the fewest monthly TA measurements (Supporting Information Table S4). Monthly mean, salinity-normalized TA (nTA, normalized to a dataset mean salinity of 29.95) was highest in January, dropped each successive month to an annual low in April, then increased to another annual high value in June (Supporting Information Table S6).

Derived parameter conditions

DIC concentrations followed the general patterns of salinity and TA, with higher DIC found at higher salinities (Fig. 2; Supporting Information Table S3). As pH is strongly affected by temperature, results of pH at in-situ temperature ($pH_{in\ situ}$) were quite different, with the lowest $pH_{in\ situ}$ in September and the highest $pH_{in\ situ}$ in March. β–H was highest, and thus buffering was strongest, in August and weakest in April. Monthly mean, salinity-normalized DIC (nDIC, normalized to a dataset mean salinity of 29.95) was highest in January and February and lowest in April in a similar pattern to nTA.

Discussion

TA and DIC mixing

Linear regression of all the CML TA measurements against salinity (Fig. 3) yielded a regression slope of 53.8 (0.2) and zero-salinity intercept (TA_0, Eq. 2) of 442 μmol kg^1 (6 μmol kg^1), with a root mean square error (RMSE) of 34.8 μmol kg^1 (r^2 0.87, p $\ll$ 0.001). There was also a strong linear relationship between DIC and salinity (Fig. 3), with a regression slope of 50.3 (0.2) and zero-salinity intercept (DIC_0, Eq. 3) of 428 μmol kg^1 (6 μmol kg^1), with an RMSE of 36.4 μmol kg^1 (r^2 0.84, p $\ll$ 0.001). The relatively high RMSE values indicate that there was considerable variability in the TA–salinity and DIC–salinity relationships at CML, either
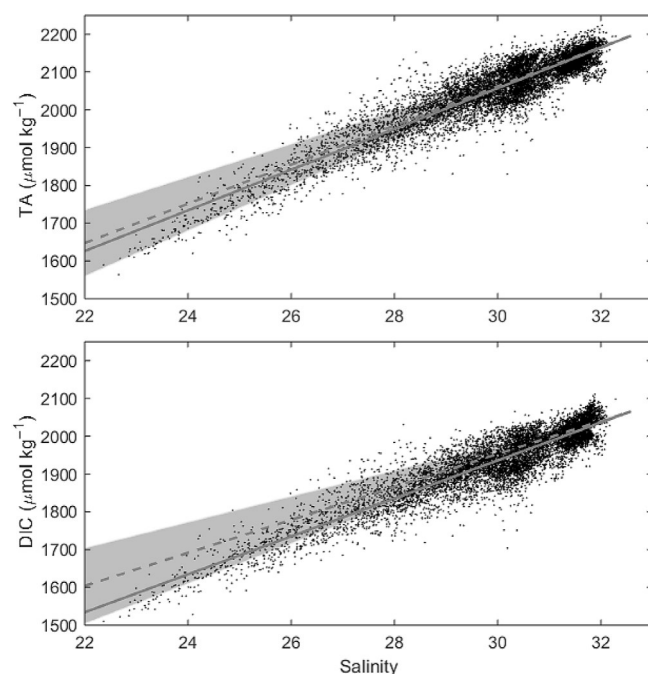

Fig. 3. CML TA (top panel) and DIC (bottom panel) distributions with salinity for data collected from 2016 to 2019. The TA measurements were made by the HydroFIA® TA instrument, while DIC was derived from measured TA and pCO_2 (refer to the text for the calculation description). The solid gray lines show the linear regression of all TA or DIC observations against salinity. The dotted gray lines show the conservative mixing of mean river TA or DIC from Hunt et al. (2011a) with a coastal ocean endmember (calculated as the TA or DIC from the solid linear regression line at the maximum observed salinity of 32.58). The gray shaded area represents the upper and lower bounds of river and coastal ocean conservative mixing. The bounds for the river endmembers were defined as one standard deviation above and below the mean TA and DIC for the three Great Bay rivers reported by Hunt et al. (2011a), while the bounds for the ocean endmember were obtained from subsurface samples collected offshore of the study site.

due to changes in water mass mixing, biogeochemical processes, or (in the case of DIC) air–sea exchange. This is evident in Fig. 4, as considerable scatter of TA and DIC both above and below the linear regression lines. To set reasonable bounds of how much of this variability might be due to variable river mixing, we used the river endmember data reported by Hunt et al. (2011a) for three rivers draining to Great Bay to estimate the mean and one standard deviation uncertainty of river TA (507 270 μmol kg^1) and DIC (644 308 μmol kg^1). These means and uncertainties easily encompass the mean TA (507 152 μmol kg^1) and DIC (500 148 μmol kg^1) mea-sured in a study of the Oyster River, which drains to Great Bay (Hunt et al. 2011b). Upper and lower conservative river mixing bounds were thus calculated using the values of Hunt et al. (2011a) and a theoretical ocean endmember calculated from the linear regression of all the TA and DIC observa-tions (Fig. 3).

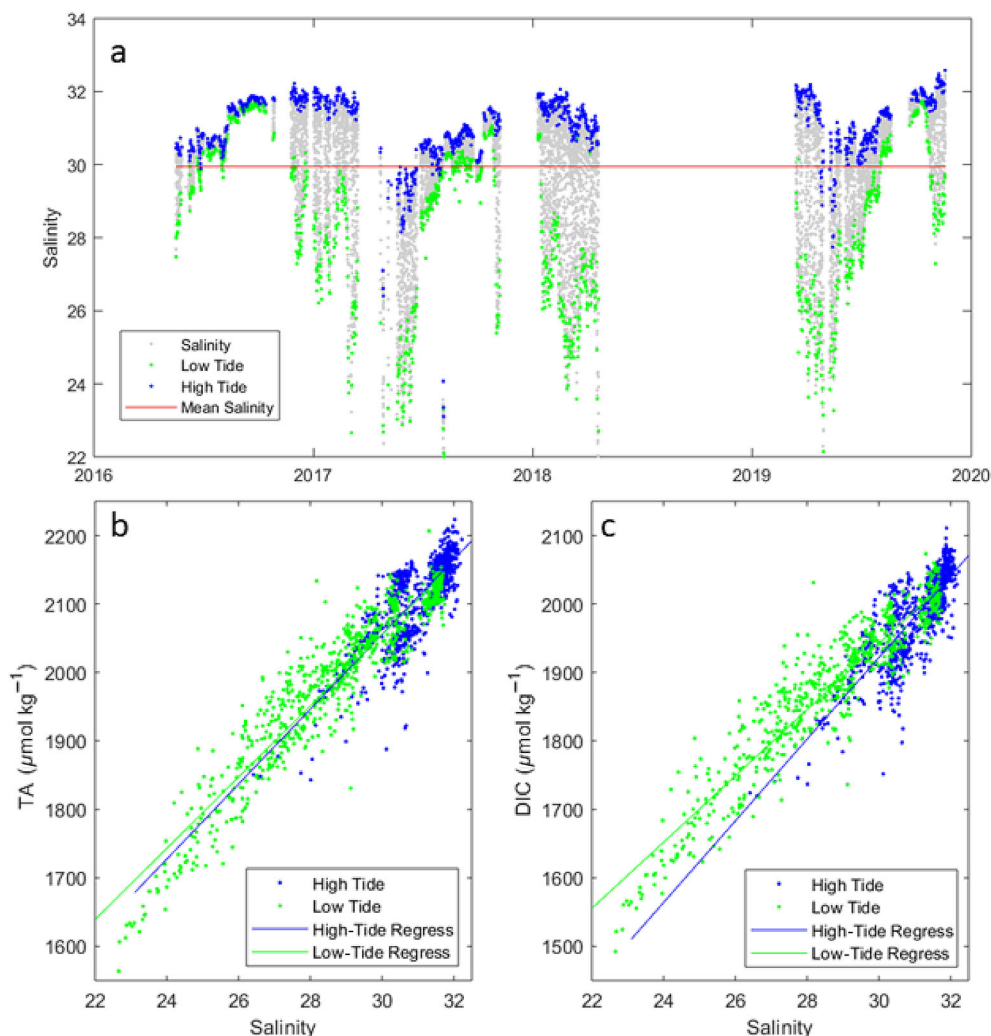A number of studies have shown that river TA and DIC concentrations vary considerably with season and discharge,

Fig. 4. CML salinity time series (a) with high-tide readings shown in blue, low-tide readings shown in green, and mid-tide readings shown in gray. See the text for discussion regarding the identification of high- and low-tide points. The linear regression of salinity against high- and low-tide TA is shown in (b). the regression equation for high-tide TA against salinity is $TA_{high\ tide} = Sx54.7\,(1.4) + 415\,(43)$ with $r^2 = 0.65$; that for the low-tide TA is $TA_{low\ tide} = Sx52.0\,(0.6) + 495\,(18)$ with $r^2 = 0.89$. The linear regression of salinity against high- and low-tide DIC is shown in (c). The regression equation for high-tide DIC against salinity is $DIC_{high\ tide} = Sx59.6\,(1.5) + 133\,(47)$ with $r^2 = 0.68$; that for the low-tide DIC is $DIC_{low\ tide} = Sx48.3\,(0.6) + 492\,(18)$ with $r^2 = 0.89$.

leading to a range of river-ocean mixing lines (Hunt et al. 2011b; Joesoef et al. 2017; Najjar et al. 2020). Although this was likely true in the CML data as well, and thus some amount of the variability of TA and DIC above and below the river mixing lines in Fig. 4 was due to changing river endmember TA and DIC, a substantial number of TA and DIC observations at CML were still above or below the bounds of this theoretical river mixing. This indicates that some of the TA and DIC variability is likely due to another process or combination of processes in addition to conservative river mixing. Another indication of estuary modification of TA and DIC was the finding that the regressed CML TA_0 was higher than the regressed DIC_0. In contrast, measured river DIC was always higher than the corresponding river TA (Hunt et al. 2011a,b).

Although the TA_0 was slightly lower than the mean river TA (507 µmol kg[1]), the DIC_0 was substantially lower than mean river DIC (644 µmol kg[1]). This discrepancy supports the idea that river-borne TA and DIC are processed non-conservatively and in different proportions in Great Bay before reaching CML. Specifically, while there may be a small amount of overall TA removal, the amount of DIC removal appears to be much larger.

Seasonal changes in TA and DIC mixing patterns

The hourly measurement rate at CML allowed for highly resolved data collection over long periods of time. To examine temporal shifts in the conservative mixing of TA and DIC with respect to salinity, we constructed monthly linear regressions

for the 27 months with sufficient data collection from 2016 to 2019 (Supporting Information Table S4). Of these 27 months, 19 TA–salinity regressions returned zero-salinity intercepts that were within the TA river-mixing bounds discussed previously, while 16 months had DIC–salinity regressions with zero-salinity intercepts that were within the DIC river-mixing bounds. The TA-salinity slope was higher than the corresponding DIC-salinity slope for 22 of the 27 months in Supporting Information Table S4, again indicating stronger estuary removal or decreases of DIC. The mean TA–salinity slope was similar to the slope of 65.8 described by Cai et al. (2010) for a transect whose inshore leg began very near CML in August 2007. However, Cai et al. (2010) reported a zero-salinity TA intercept of 188.7 $\mu mol\ kg^1$, a value which clearly requires some mechanism of TA removal to explain.

The strongest linear correlations between TA or DIC and salinity, according to the r^2 statistic, tended to be in the winter (December, January, February) and spring months (March and May), while the weaker r^2 statistics in summer and fall months indicated that mixing was less conservative. The winter and spring months also tended to have TA–salinity regression slopes near the mean value (60.0), while the summer and fall months showed widely varying TA–salinity slopes (ranging from 5.0 to 150). However, it should be noted that the summer and fall months were also those with lowest river flow and salinity variability, and therefore the less robust salinity mixing relationships for these months were not surprising. For example, in September 2016 the salinity variability was only 0.5; considering the overall mean TA-salinity slope of 53.8 this translated into a potential TA variability of half the slope, or 26.9 $\mu mol\ kg^1$. This was only somewhat higher that the overall uncertainty in the TA instrument accuracy (18 $\mu mol\ kg^1$), indicating that in months of very low-salinity variability the TA instrument may not be capable of determining a meaningful TA–salinity relationship. But it is worth noting that while the overall accuracy uncertainty over the study period was 18 $\mu mol\ kg^1$, in September 2016 the uncertainty in instrument accuracy was lower (11 $\mu mol\ kg^1$, n = 3), allowing for meaningful interpretation of the results despite the small salinity changes in this and other months (Supporting Information Fig. S1). Despite the added uncertainty in TA–salinity and DIC–salinity regressions in the summer and fall months, there appeared to be other factors contributing to TA and DIC observations.

High- and low-tide TA and DIC

Tidal exchanges between the coastal ocean and Great Bay are very strong, funneling large volumes of water past CML over each diurnal cycle. One study estimated a Great Bay flushing time of 2.5–7 d (Matso 2018), while another gave a range of 5–30 d depending on tidal stage and river discharge (Bilgili et al. 2005). Both studies show that much of the water in Great Bay is replaced over each tide. As the predominant

coastal flow outside of CML is southward (Townsend et al. 2006), the water which passes CML on the incoming tide is mostly advected south on the subsequent outgoing tide instead of re-entering Great Bay on the next tide. Therefore, we suggest that a simplistic conceptual model for each tidal cycle can be represented by "newer" coastal water entering the estuary past CML on the incoming tide, mixing with a pool of estuary water comprised of a combination of river and "older" coastal water, and then exiting past CML again on the outgoing tide. Thus high tide presumably represents the greatest fraction of coastal water, and low tide represents the greatest fraction of mixed estuary water. We used salinity to identify high and low tides (as opposed to the observed tidal stage height) and the corresponding high- and low-tide TA and DIC (Fig. 4) by first identifying the lowest salinity measurement within a 7-h time frame of data ("findpeaks," MATLAB, Mathworks), then searching the previous 9 h for the highest salinity. We chose to employ this strategy due to a mismatch between the time of lowest tidal height and the time of lowest salinity, where the lowest salinity was observed multiple hours after the lowest tidal height observation. This apparent asymmetry between tidal elevation and salinity is due to the dissipation of the energy of the tidal wave as it moves past CML and proceeds upstream, resulting in the phase of the tidal flow lagging that of the elevation (T. Lippmann pers. comm.). Although our salinity-based identification method did not strictly correspond to the technical definitions of high and low tides relative to sea surface height, we will use the common terms high and low tide henceforth to refer to the times of highest and lowest salinity during each diurnal tidal cycle.

Linear regression of high- and low-tide TA against salinity yielded statistically similar results (Fig. 4), indicating that there did not appear to be a significant change in TA in the water leaving Great Bay past CML on the outgoing tide relative to water entering past CML on the incoming tide. In addition, the TA_0 for high and low tides (415 43 $\mu mol\ kg^1$ and 495 18 $\mu mol\ kg^1$, respectively) were well within the wide river endmember TA range (507 270 $\mu mol\ kg^1$). However, linear regression of DIC against salinity produced different regression lines for high and low tide, with the low-tide DIC having a shallower linear slope and higher DIC_0 than those from the high-tide measurements, indicating a relative input of DIC to the water leaving Great Bay past CML on the outgoing tide. The low-tide DIC_0 (492 18 $\mu mol\ kg^1$) is also much closer to the approximate river endmember DIC (644 308 $\mu mol\ kg^1$) than the corresponding high-tide DIC_0 (133 47 $\mu mol\ kg^1$).

Contributions of mixing and temperature to buffering and pH

A simple set of calculations were performed to examine the relative influence of TA and DIC mixing and seasonal temperature changes on β–H and pH. Each parameter was calculated

using CO2SYS, with TA and DIC inputs determined from the dataset-wide relationships with salinity (Fig. 3). The mixing influence was determined using a constant water temperature

Fig. 5. Observed monthly mean buffer factor β–H (top panel) and pH (bottom panel), indicated by the solid black line. Error bars indicate plus and minus one standard deviation of monthly mean β–H or pH. Mean annual β–H (352 μmol kg[1]) and pH (7.96) are shown as dashed black lines. Theoretical β–H ("β–H MIX, β–H TEMP") and pH ("pH MIX, pH TEMP") due to endmember mixing and temperature changes, calculated from whole-dataset salinity–TA and salinity–DIC regressions, mean monthly salinity, and mean monthly temperature, are shown as solid blue and red lines for MIX and TEMP, respectively. β–H and pH from the combined effects of MIX and TEMP are shown as dashed green lines.

of 10C, monthly mean salinity (Supporting Information Table S2), and conservatively mixed TA and DIC (Supporting Information Fig. 3). The temperature influence was determined using mean monthly temperature (Supporting Information Table S2) and a dataset-wide mean salinity of 29.9, TA of 2048 μmol kg[1], and DIC of 1931 μmol kg[1]. Application of the monthly mixing and temperature effects to mean β–H (352 μmol kg[1]) and pH (7.96) showed that mixing and temperature respectively account for much of the annual variability in β–H and pH at this site (Fig. 5). The mean mixing effect was about three times stronger than the mean temperature effect for β–H (9.4 and 2.4 μmol kg[1], respectively), while the temperature effect was nearly an order of magnitude stronger than the mixing effect for pH (0.06 and 0.007, respectively). Although $pH_{in\ situ}$ and water temperature are expected to vary inversely, lower pH_{25C} values in the fall emphasized that temperature was not the only factor contributing to the pH changes.

Relative influences of mixing and NEM on TA and DIC

Both mixing and NEM contributed to changes in TA, DIC, pH, and β–H, and these contributions appeared to shift seasonally, with mixing processes (and temperature) controlling changes for much of the year as shown in Fig. 5, but metabolic process signatures were also evident in the late summer and fall (Fig. 6). Results from a deterministic model (Fig. 7) help explain the apparent contradiction that β–H was highest in late summer and fall while this period also showed the largest change in nTA : nDIC that implied enhanced metabolic activity. Overall, the model showed that mixing was the dominant control on changes in DIC and TA in winter and spring, a model result that is mostly driven by the higher degree of salinity variability (Fig. 2; Supporting Information Table S2). By June the salinity became much less variable, and NEM overtook mixing as the more significant control. Air–sea flux,
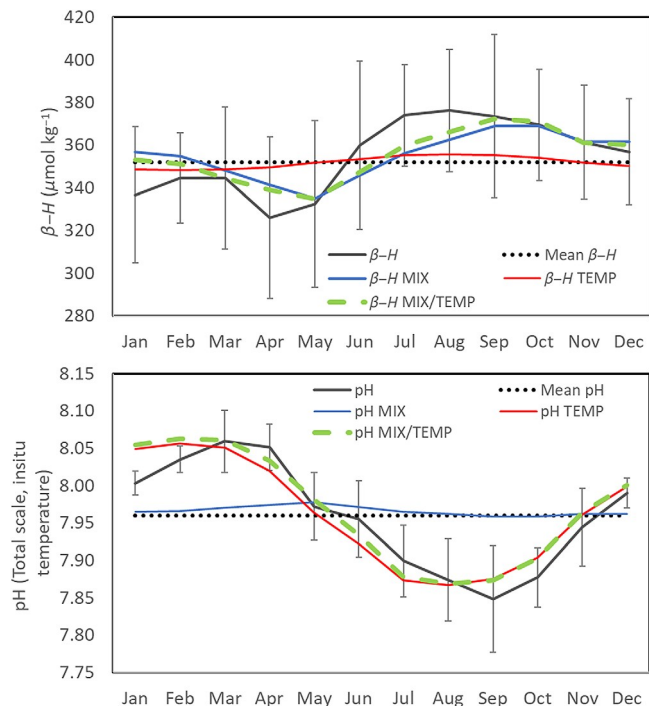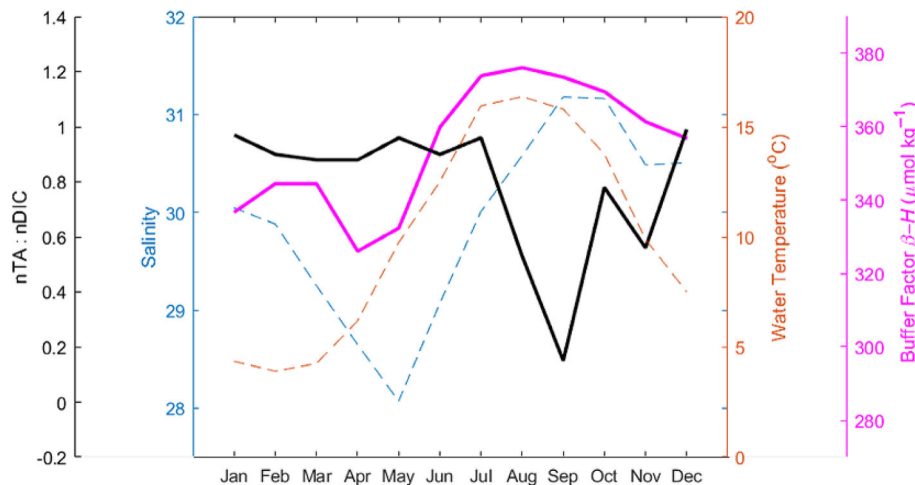

Fig. 6. Monthly climatological salinity (dashed blue line), water temperature (dashed red line), buffer factor β–H (solid magenta line), and nTA : nDIC slope (solid black line) at the CML, calculated using data from 2016 through 2019.

which only influences changes in DIC, also increased in importance through the summer, becoming the largest factor influencing DIC in the months of August and October. Interestingly, the model showed some summer and late fall months (August, October, and November) exhibited diminished NEM influence on DIC relative to the spring and early summer, but this decrease in NEM was smaller than the decrease in mixing. The decreased mixing influence was due to less freshwater entering the estuary, resulting in saltier conditions at CML and relatively high salinities at both low and high tides, with proportionally higher DIC and TA. This then led to a more strongly buffered system despite the relatively strong influence of NEM. It is worth noting that some metabolic activity may be reflected in the seasonal changes in the ocean mixing endmember (Supporting Information Fig. S2), and thus some of the mixing contribution at CML may instead be reflective of remote coastal ocean NEM. Whereas some studies show that metabolic processes may pose a significant acidification risk in low-oxygen estuary waters (Cai et al. 2017; Van Dam and Wang 2019), others have indicated that well-mixed estuary waters may actually be buffered by increased NEM (Nixon et al. 2015). These results suggest that NEM at CML represents a smaller acidification risk than changes to river inputs of TA and DIC (Salisbury et al. 2008) or acidification controlled by the coastal ocean. We emphasize here that these findings from CML, located at the mouth of the estuary, may not apply to conditions in Great Bay itself. Oxygen and pH monitoring data at CML and in central Great Bay surface waters do not show especially low oxygen or pH levels (PREP 2017; NERR 2021). However, the same oxygen and pH levels in three of the primary tidal rivers supplying Great Bay (the Oyster, Lamprey, and Squamscott rivers, Fig. 1) can be much lower, with frequent evidence of hypoxia and low pH which may be promoted by NEP (PREP 2017, NERR 2021). Although efforts to mitigate OCA by reducing nutrient inputs to lower overall NEM may be beneficial in Great Bay, they may have a lesser effect at CML.

Biogeochemical processes affecting TA and DIC

As discussed earlier, conservative river-ocean TA mixing models are often used to estimate TA distributions in estuaries, and during the winter and spring seasons in Great Bay conservative mixing does appear to explain the general TA distributions with salinity (Fig. 3; Supporting Information Table S4). But estuaries can also be sites of intense biogeochemical processing, especially of allochthonous and autochthonous organic matter, which can alter TA, DIC, or both in varying proportions, depending on the stoichiometry of the chemical reaction or reactions that predominate (Borges et al. 2003; Bouillon et al. 2007; Krumins et al. 2013; Sippo et al. 2016; Cai et al. 2017). Some common processes and their ΔDIC : ΔTA ratios are discussed by Cai et al. (2017) and Sippo et al. (2016) and summarized in Supporting Information
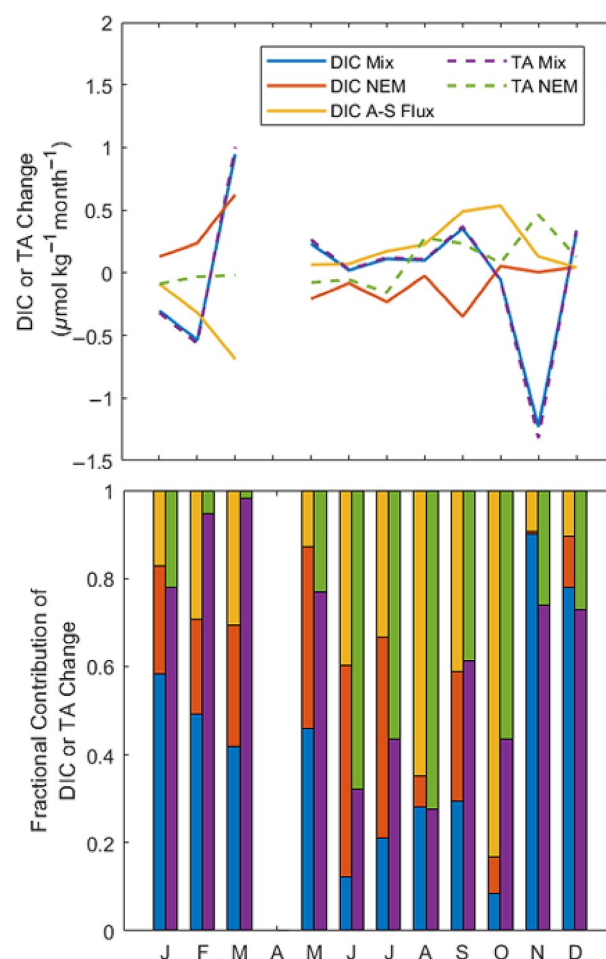

Fig. 7. Modeled, monthly mean changes in DIC and TA due to mixing, metabolic and air-sea flux processes (top panel) and relative contributions of these processes to the total monthly DIC or TA change (bottom panel). Values shown in the top panel are the monthly mean values of DIC and TA changes over each hourly time step. The colors of lines shown in the legend of the top panel correspond to the bar colors of the bottom panel. Note that the DIC mix and TA mix lines in the top panel virtually overlie one another, and that results from April are excluded due to low data availability as discussed in the text.

Table S5. Aerobic respiration or primary production can occur in the pelagic environment or the oxygenated benthos, while the remaining processes are components of complex anaerobic biogeochemical cycling within estuarine and coastal sediments that is subsequently reflected in the overlying water, where aerobic respiration/primary production, sulfate reduction, carbonate dissolution or precipitation, and denitrification tend to predominate in most coastal basins (Burdige 2011; Ulfsbo et al. 2011; Hagens et al. 2015). These processes may occur simultaneously or be coupled together to transport electrons through various sediment layers, and the linkage between sediment chemistry and the chemistry of the overlying water is complex and may depend on a variety of physical and biogeochemical factors beyond the processes listed in Supporting Information Table S5 (Burdige 2011;
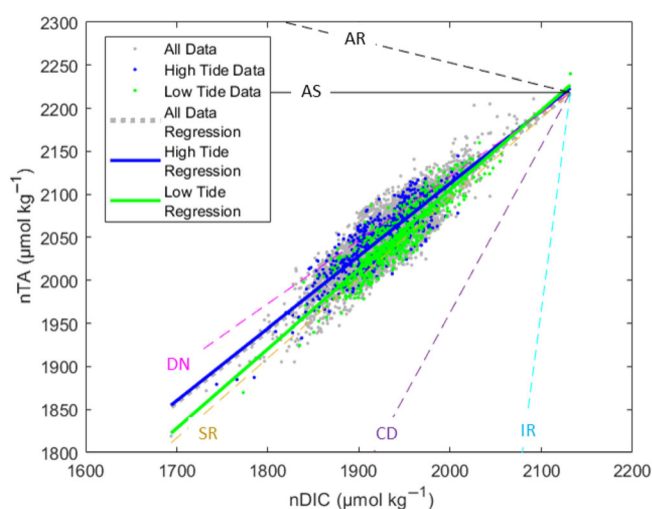
Fig. 8. All salinity-normalized DIC (nDIC) and salinity-normalized TA (nTA) from the CML observations (gray points), with high-tide data (blue points) and low-tide data (green points) corresponding to those shown in Fig. 4. Dashed lines show the stoichiometric nTA : nDIC changes for common estuarine processes: aerobic respiration (AR), air–sea CO_2 exchange (AS), denitrification (DN), sulfate reduction (SR), carbonate dissolution (CD), and iron reduction (IR), are provided as reference and do not indicate controlling processes in this study. The solid blue line shows the lin-ear regression of high-tide data points (slope 0.84 0.017), while the solid green line shows that of low-tide data points (slope 0.92 0.016). The linear regression of all data (dashed gray line, slope 0.83 0.005) is essentially covered by the solid blue high-tide regression line.

Brenner et al. 2016; Cai et al. 2017; Gustafsson et al. 2019). This study did not include other measurements including pore water chemistry, nitrogen or phosphorus species, hydrogen sulfide concentrations, or calcification rates, which are needed to thoroughly examine the prevalence of specific biogeochemical processes, and thus we simply present our observations with the processes listed in Supporting Information Table S5 intended as a reference.

The linear regression of all salinity-normalized TA against salinity-normalized DIC (nTA and nDIC respectively, normalized to a S_{mean} of 29.95, Fig. 8) yielded a nTA : nDIC slope of 0.83 0.005. Although the overall CML nTA : nDIC regres-sion was linear (r^2 0.75, $p < 0.001$), there was significant scatter around the regression line (nTA RMSE 18 μmol kg^1). Examination of the nTA : nDIC distributions at high and low tides showed clear differences (Fig. 8). The high-tide slope (0.84 0.017, $r^2 = 0.77$, $p < 0.001$) was indistinguishable from the overall trend of all data. The low-tide slope (0.92 0.016, $r^2 = 0.83$, $p < 0.001$), however, was significantly steeper than the high-tide slope, perhaps indicating that biogeochemical processing was a stronger contributor at low tide, a logical result as the tidal flushing out of Great Bay and past CML and consequent sea height drop results in more benthic–pelagic interaction.

In addition to differences in the nTA : nDIC slope between high and low tides, there was also a seasonal progression of

nTA : nDIC slope (Fig. 6). Monthly nTA : nDIC slopes were generally between 0.8 and 1.0, excepting a large decrease in the later summer and fall months (August through October). These months were also the months of least-linear nTA : nDIC as indicated by generally low r^2 values (Supporting Information Table S4). This general pattern was seen across years between 2016 and 2019 with some interannual variability. Although there were differences between low and high tides monthly nTA : nDIC slopes, these differences were small and inconsistent between years.

It is worthwhile to consider how river-ocean mixing might also affect the TA : DIC signature. A limited dataset of TA and DIC from three Great Bay rivers exhibited a mean TA : DIC of 0.78 (0.11, n = 12; Hunt et al. 2011a), while a more exten-sive time series of data from one Great Bay river (the Oyster River) exhibited a mean TA : DIC of 1.02 (0.14, n = 41; Hunt et al. 2011b). Thus TA : DIC data from Great Bay rivers encompass the nTA : nDIC values seen at both high and low tides at CML. A simple endmember mixing calculation (not shown) determined that variability in river TA : DIC probably has little effect on the nTA : nDIC slopes at CML, and that other processes must be present.

Conclusions

This study presents evidence that CML, at the outlet of Great Bay, is a site of dynamic mixing which influences estu-ary buffering capacity and acidification potential. Biogeochemical processes such as primary productivity and aerobic respiration may contribute to annual changes in pH, pCO_2, DIC, and β–H but the signatures of these processes are difficult to discern within the strong mixing and temperature signals. The late summer and fall, when biogeochemical processes have the strongest influence on changes in TA and DIC, is also the period when the estuary is most highly buffered by an abundance of high-salinity water. Future work could include estuary sampling transects from CML through Great Bay, with concurrent river endmember sampling. This would provide a snapshot of TA and DIC addition relative to conservative mixing along the salinity gradient over a short time period and may identify areas upstream of CML where biogeochemical process signatures are discernible from physical controls. These next steps would produce findings useful to policy makers and coastal managers who will need to decide which processes may be affected by regulation in order to better monitor and potentially ameliorate OCA.

References

Bauer, J. E., W.-J. Cai, P. A. Raymond, T. S. Bianchi, C. S. Hopkinson, and P. A. G. Regnier. 2013. The changing carbon cycle of the coastal ocean. Nature 504: 61–70. doi:10.1038/nature12857

Bilgili, A., J. A. Proehl, D. R. Lynch, K. W. Smith, and M. R. Swift. 2005. Estuary/ocean exchange and tidal mixing in a Gulf of Maine Estuary: A Lagrangian modeling study. Estuar. Coast. Shelf Sci. 65: 607–624. doi:10.1016/j.ecss.2005.06.027

Borges, A. V., S. Djenidi, G. Lacroix, J. Théate, B. Delille, and M. Frankignoulle. 2003. Atmospheric CO_2 flux from mangrove surrounding waters. Geophys. Res. Lett. 30: 1558. doi:10.1029/2003GL017143

Borges, A. V. 2005. Do we have enough pieces of the jigsaw to integrate CO_2 fluxes in the coastal ocean? Estuaries 28: 3–27. doi:10.1007/BF02732750

Bouillon, S., F. Dehairs, B. Velimirov, G. Abril, and A. V. Borges. 2007. Dynamics of organic and inorganic carbon across contiguous mangrove and seagrass systems (Gazi Bay, Kenya). J. Geophys. Res. 112: G02018. doi:10.1029/2006JG000325

Brenner, H., U. Braeckman, M. Le Guitton, and F. J. R. Meysman. 2016. The impact of sedimentary alkalinity release on the water column CO_2 system in the North Sea. Biogeosciences 13: 841–863. doi:10.5194/bg-13-841-2016

Breitburg, D. L., J. Salisbury, J. M. Bernhard, and others. 2015. And on top of all that…: Coping with ocean acidification in the midst of many stressors. Oceanography 28: 48–61,

Broecker, W. S., T. Takahashi, H. J. Simpson, and T.-H. Peng. 1979. Fate of fossil fuel carbon dioxide and the global carbon budget. Science 206: 409–418. doi:10.1126/science.206.4417.409

Brown, T. 2006. Non-reactive gas dynamics in the Piscataqua Estuary inlet. Univ. of New Hampshire.

Burdige, D. J. 2011. Estuarine and coastal sediments—Coupled biogeochemical cycling. Treatise Estuar. Coast. Sci. 5: 279–316.

Caffrey, J. M. 2004. Factors controlling net ecosystem metabolism in U.S. estuaries. Estuaries 27: 90–101. doi:10.1007/BF02803563

Cai, W.-J., and Y. Wang. 1998. The chemistry, fluxes, and sources of carbon dioxide in the estuarine waters of the Satilla and Altamaha Rivers, Georgia. Limnol. Oceanogr. 43: 657–668. doi:10.4319/lo.1998.43.4.0657

Cai, W.-J., Y. Wang, and R. E. Hodson. 1998. Acid–base properties of dissolved organic matter in the estuarine waters of Georgia, USA. Geochim. Cosmochim. Acta 62: 473–483. doi:10.1016/S0016-7037(97)00363-3

Cai, W.-J., X. Hu, W.-J. Huang, L.-Q. Jiang, Y. Wang, T.-H. Peng, and X. Zhang. 2010. Alkalinity distribution in the western North Atlantic Ocean margins. J. Geophys. Res. 115: C08014. doi:10.1029/2009JC005482

Cai, W.-J., and others. 2017. Redox reactions and weak buffering capacity lead to acidification in the Chesapeake Bay. Nat. Commun. 8: 369. doi:10.1038/s41467-017-00417-7

Cai, W.-J., and others. 2020. Natural and anthropogenic drivers of acidification in large estuaries. Annu. Rev. Mar. Sci. doi:10.1146/annurev-marine-010419-011004.

COMNARE (NH Coastal Marine Natural Resources & Environment Commission). 2017. 2017 Annual report—Ocean acidification summary and recommendations. [Accessed 2021 February 12]. https://mypages.unh.edu/sites/default/files/comnare/files/comnare_2017_report_to_state.pdf

Cook, S. 2019. Effects of waves, tides, and vegetation on the distribution of bed shear stress in the Great Bay Estuary, NH. Doctoral dissertations 2485. Available from https://scholars.unh.edu/dissertation/2485

De Meo, O. 2011. Studies of net community productivity in a near-coastal temperate ecosystem. Univ. of New Hampshire.

Dickson, A. G. 1990. Thermodynamics of the dissociation of boric acid in synthetic seawater from 273.15 to 318.15 K. Deep Sea Res. Part A Oceanogr. Res. Pap. 37: 755–766. doi:10.1016/0198-0149(90)90004-F

Dickson, A. G., D. J. Wesolowski, D. A. Palmer, and R. E. Mesmer. 1990. Dissociation constant of bisulfate ion in aqueous sodium chloride solutions to 250C. J. Phys. Chem. 94: 7978–7985. doi:10.1021/j100383a042

Dickson, A. G., J. D. Afghan, and G. C. Anderson. 2003. Reference materials for oceanic CO_2 analysis: A method for the certification of total alkalinity. Mar. Chem. 80: 185–197. doi:10.1016/S0304-4203(02)00133-0

Dickson, A. G., C. L. Sabine, and J. R. Christian [eds.]. 2007. Guide to best practices for ocean CO_2 measurements. PICES Special Publication 3. North Pacific Marine Science Organization.

Doney, S. C., N. Mahowald, I. Lima, R. A. Feely, F. T. Mackenzie, J.-F. Lamarque, and P. J. Rasch. 2007. Impact of anthropogenic atmospheric nitrogen and sulfur deposition on ocean acidification and the inorganic carbon system. PNAS 104: 14580–14585. doi:10.1073/pnas.0702218104

Doney, S. C., V. J. Fabry, R. A. Feely, and J. A. Kleypas. 2009. Ocean acidification: The other CO2 problem. Ann. Rev. Mar. Sci. 1: 169–192. doi:10.1146/annurev.marine.010908.163834

Driscoll, C. T., and others. 2001. Acidic deposition in the northeastern United States: Sources and inputs, ecosystem effects, and management strategies: The effects of acidic deposition in the northeastern United States include the acidification of soil and water, which stresses terrestrial and aquatic biota. Bioscience 51: 180–198 doi:10.1641/0006-3568(2001)051[0180:ADITNU]2.0.CO;2.

Duarte, C. M., and others. 2013. Is ocean acidification an open-ocean syndrome? Understanding anthropogenic impacts on seawater pH. Estuar. Coasts 36: 221–236. doi:10.1007/s12237-013-9594-3,

Egleston, E. S., C. L. Sabine, and F. M. M. Morel. 2010. Revelle revisited: Buffer factors that quantify the response of ocean

chemistry to changes in DIC and alkalinity. Global Bio-geochem. Cycl. 24: GB1002. doi:10.1029/2008GB003407

Faber, P. A., V. Evrard, R. J. Woodland, I. C. Cartwright, and P. L. M. Cook. 2014. Pore-water exchange driven by tidal pumping causes alkalinity export in two intertidal inlets. Limnol. Oceanogr. 59: 1749–1763. doi:10.4319/lo.2014.59.5.1749

Fennel, K., J. Wilkin, M. Previdi, and R. Najjar. 2008. Denitrification effects on air-sea CO_2 flux in the coastal ocean: Simulations for the northwest North Atlantic. Geophys. Res. Lett. 35: L24608. doi:10.1029/2008GL036147

Friis, K., A. Körtzinger, and D. W. R. Wallace. 2003. The salinity normalization of marine inorganic carbon chemistry data. Geophys. Res. Lett. 30: 1085. doi:10.1029/2002GL015898

Gattuso, J.-P., M. Frankignoulle, and R. Wollast. 1998. Carbon and carbonate metabolism in coastal aquatic ecosystems. Annu. Rev. Ecol. Syst. 29: 405–434. doi:10.1146/annurev.ecolsys.29.1.405

Gledhill, D., M. White, J. Salisbury, and others. 2015. Ocean and coastal acidification off New England and Nova Scotia. Oceanography 25: 182–197. doi:10.5670/oceanog.2015.41

Gustafsson, E., M. Hagens, X. Sun, D. C. Reed, C. Humborg, C. P. Slomp, and B. G. Gustafsson. 2019. Sedimentary alkalinity generation and long-term alkalinity development in the Baltic Sea. Biogeosciences 16: 437–456. doi:10.5194/bg-16-437-2019

Hagens, M., C. P. Slomp, F. J. R. Meysman, D. Seitaj, J. Harlay, A. V. Borges, and J. J. Middelburg. 2015. Biogeochemical processes and buffering capacity concurrently affect acidification in a seasonally hypoxic coastal marine basin. Biogeosciences 12: 1561–1583. doi:10.5194/bg-12-1561-2015

Hunt, C. W., J. E. Salisbury, D. Vandemark, and W. McGillis. 2011a. Contrasting carbon dioxide inputs and exchange in three adjacent New England estuaries. Estuar. Coasts 34: 68–77. doi:10.1007/s12237-010-9299-9

Hunt, C. W., J. E. Salisbury, and D. Vandemark. 2011b. Contribution of non-carbonate anions to total alkalinity and overestimation of pCO_2 in New England and New Brunswick rivers. Biogeosciences 8: 3069–3076. doi:10.5194/bg-8-3069-2011

Hunt, C. W., J. E. Salisbury, D. Vandemark, S. Aßmann, P. Fietzek, C. Melrose, R. Wanninkhof, and K. Azetsu-Scott. 2021. Variability of USA East Coast surface total alkalinity distributions revealed by automated instrument measurements. Mar. Chem. 232: 103960. doi:10.1016/j.marchem.2021.103960

IPCC. 2021. Climate change 2021: The physical science basis. In V. Masson-Delmotte and others. [eds.], Contribution of Working Group I to the Sixth Assessment Report of the Intergovernmental Panel on Climate Change. Cambridge University Press, In Press.

Joesoef, A., D. L. Kirchman, C. K. Sommerfield, and W.-J. Cai. 2017. Seasonal variability of the inorganic carbon system in a large coastal plain estuary. Biogeosciences 14: 4949–4963. doi:10.5194/bg-14-4949-2017

Jones, S. H. 2000. A technical characterization of estuarine and coastal New Hampshire. New Hampshire Estuaries Project.

Kaushal, S. S., G. E. Likens, R. M. Utz, M. L. Pace, M. Grese, and M. Yepsen. 2013. Increased river alkalinization in the Eastern U.S. Environ. Sci. Technol. 47: 10302–10311. doi:10.1021/es401046s

Kaushal, S. S., and others. 2014. Land use and climate variability amplify carbon, nutrient, and contaminant pulses: A review with management implications. J. Am. Water Resour. Assoc. 50: 585–614. doi:10.1111/jawr.12204

Krumins, V., M. Gehlen, S. Arndt, P. V. Cappellen, and P. Regnier. 2013. Dissolved inorganic carbon and alkalinity fluxes from coastal marine sediments: Model estimates for different shelf environments and sensitivity to global change. Biogeosciences 10: 371–398. doi:10.5194/bg-10-371-2013

Lee, D. Y., M. S. Owens, M. Doherty, E. M. Eggleston, I. Hewson, B. C. Crump, and J. C. Cornwell. 2015. The effects of oxygen transition on community respiration and potential chemoautotrophic production in a seasonally stratified anoxic estuary. Estuar. Coasts 38: 104–117. doi:10.1007/s12237-014-9803-8

Leopold, A., C. Marchand, J. Deborde, and M. Allenbach. 2016. Water biogeochemistry of a mangrove-dominated estuary under a semi-arid climate (New Caledonia). Estuar. Coasts 1–19: 773–791. doi:10.1007/s12237-016-0179-9

Lerczak, J. A., and W. Rockwell Geyer. 2004. Modeling the lateral circulation in straight, stratified estuaries. J. Phys. Oceanogr. 34: 1410–1428. doi:10.1175/1520-0485(2004)034<1410:MTLCIS>2.0.CO;2

Li, Q., F. Wang, Z. A. Wang, D. Yuan, M. Dai, J. Chen, J. Dai, and K. A. Hoering. 2013. Automated spectrophotometric analyzer for rapid single-point titration of seawater total alkalinity. Environ. Sci. Technol. 47: 11139–11146. doi:10.1021/es402421a

Matso, K. 2018. Flushing time versus residence time for the Great Bay Estuary. Piscataqua Region Estuaries Partnership Reports & Publications. 413. https://scholars.unh.edu/prep/413.

Middelburg, J. J., K. Soetaert, and M. Hagens. 2020. Ocean alkalinity, buffering and biogeochemical processes. Rev. Geophys. 58: e2019RG000681. doi:10.1029/2019RG000681

Millero, F. J., K. Lee, and M. Roche. 1998. Distribution of alkalinity in the surface waters of the major oceans. Mar. Chem. 60: 111–130. doi:10.1016/S0304-4203(97)00084-4

MSLCOOA, Massachusetts Special Legislative Commission on Ocean Acidification. 2021. Report on the ocean acidification crisis in Massachusetts. 84 pp. [Accessed 2021 February 12]. https://www.mass.gov/files/documents/2021/12/15/massachusetts-ocean-acidification-report-feb-2021.pdf

Najjar, R. G., M. Herrmann, S. M. C. D. Valle, and others. 2020. Alkalinity in tidal tributaries of the Chesapeake Bay.

J. Geophys. Res. Oceans 125: e2019JC015597. doi:10.1029/2019JC015597,

NERR (National Estuarine Research Reserve). 2021. Centralized data management office. [Accessed 2021 April 21]. https://cdmo.baruch.sc.edu/dges/

Nixon, S. W., A. J. Oczkowski, M. E. Q. Pilson, L. Fields, C. A. Oviatt, and C. W. Hunt. 2015. On the response of pH to inorganic nutrient enrichment in well-mixed coastal marine waters. Estuar. Coasts 38: 232–241. doi:10.1007/s12237-014-9805-6

Orr, J. C., V. J. Fabry, O. Aumont, and others. 2005. Anthropogenic ocean acidification over the twenty-first century and its impact on calcifying organisms. Nature 437: 681–686. doi:10.1038/nature04095,

Pacella, S. R., C. A. Brown, G. G. Waldbusser, R. G. Labiosa, and B. Hales. 2018. Seagrass habitat metabolism increases short-term extremes and long-term offset of CO2 under future ocean acidification. PNAS 115: 3870–3875. doi:10.1073/pnas.1703445115

PREP (Piscataqua Region Estuaries Partnership). 2017. State of our estuaries report 2018. PREP Reports & Publications. 391. https://www.stateofourestuaries.org/2018-reports/sooe-full-report.

Raymond, P. A., J. E. Bauer, and J. J. Cole. 2000. Atmospheric CO_2 evasion, dissolved inorganic carbon production, and net heterotrophy in the York River estuary. Limnol. Oceanogr. 45: 1707–1717. doi:10.4319/lo.2000.45.8.1707

Rheuban, J. E., S. C. Doney, D. C. McCorkle, and R. W. Jakuba. 2019. Quantifying the effects of nutrient enrichment and freshwater mixing on Coastal Ocean acidification. J. Geophys. Res. Oceans 124: 9085–9100. doi:10.1029/2019JC015556

Salisbury, J., M. Green, C. Hunt, and J. Campbell. 2008. Coastal acidification by rivers: A threat to shellfish? Eos Trans. AGU 89: 513. doi:10.1029/2008EO500001

Seelmann, K., S. Aßmann, and A. Körtzinger. 2019. Characterization of a novel autonomous analyzer for seawater total alkalinity: Results from laboratory and field tests. Limnol. Oceanogr. Methods 17: 515–532. doi:10.1002/lom3.10329

Sharp, J. D., and R. H. Byrne. 2021. Technical note: Excess alkalinity in carbonate system reference materials. Mar. Chem. 233: 103965. doi:10.1016/j.marchem.2021.103965

Short, F. T. 1992. The ecology of the Great Bay estuary, New Hampshire and Maine: An estuarine profile and bibliography. Univ. of New Hampshire.

Sippo, J. Z., D. T. Maher, D. R. Tait, C. Holloway, and I. R. Santos. 2016. Are mangroves drivers or buffers of coastal acidification? Insights from alkalinity and dissolved inorganic carbon export estimates across a latitudinal transect. Global Biogeochem. Cycl. 30: 2015GB005324. doi:10.1002/2015GB005324

Townsend, D. W., A. C. Thomas, L. M. Mayer, M. Thomas, and J. Quinlan. 2006. Oceanography of the Northwest Atlantic continental shelf, p. 119–168. In The sea. Harvard Univ. Press.

Ulfsbo, A., S. Hulth, and L. G. Anderson. 2011. pH and biogeochemical processes in the Gotland Basin of the Baltic Sea. Mar. Chem. 127: 20–30. doi:10.1016/j.marchem.2011.07.004

Uppström, L. R. 1974. The boron/chlorinity ratio of deep-sea water from the Pacific Ocean. Deep-Sea Res. Oceanogr. Abstr. 21: 161–162. doi:10.1016/0011-7471(74)90074-6

Van Dam, B. R., and H. Wang. 2019. Decadal-scale acidification trends in adjacent North Carolina estuaries: Competing role of anthropogenic CO_2 and riverine alkalinity loads. Front. Mar. Sci. 6. doi:10.3389/fmars.2019.00136

van Heuven, S., D. Pierrot, J. W. B. Rae, E. Lewis, and D. W. R. Wallace. 2011. CO2SYS v 1.1. MATLAB program developed for CO_2 system calculations. ORNL/CDIAC-105b. ORNL/CDIAC-105b. Oak Ridge National Laboratory, U.S. Department of Energy.

Waldbusser, G. G., E. N. Powell, and R. Mann. 2013. Ecosystem effects of shell aggregations and cycling in coastal waters: An example of Chesapeake Bay oyster reefs. Ecology 94: 895–903. doi:10.1890/12-1179.1

Waldbusser, G., and J. Salisbury. 2014. Ocean acidification in the coastal zone from an organism's perspective: Multiple system parameters, frequency domains, and habitats. Ann. Rev. Mar. Sci. 6: 221–247. doi:10.1146/annurev-marine-121211-172238

Wang, Z. A., and W.-J. Cai. 2004. Carbon dioxide degassing and inorganic carbon export from a marsh-dominated estuary (the Duplin River): A marsh CO_2 pump. Limnol. Oceanogr. 49: 341–354. doi:10.4319/lo.2004.49.2.0341

Wang, G., W. Jing, S. Wang, Y. Xu, Z. Wang, Z. Zhang, Q. Li, and M. Dai. 2014. Coastal acidification induced by tidal-driven submarine groundwater discharge in a coastal coral reef system. Environ. Sci. Technol. 48: 13069–13075. doi:10.1021/es5026867

Wang, Z. A., K. D. Kroeger, N. K. Ganju, M. E. Gonneea, and S. N. Chu. 2016. Intertidal salt marshes as an important source of inorganic carbon to the coastal ocean. Limnol. Oceanogr. 61: 1916–1931. doi:10.1002/lno.10347

Wanninkhof, R., and K. Thoning. 1993. Measurement of fugacity of CO_2 in surface water using continuous and discrete sampling methods. Mar. Chem. 44: 189–204. doi:10.1016/0304-4203(93)90202-Y

Yang, B., R. H. Byrne, and M. Lindemuth. 2015. Contributions of organic alkalinity to total alkalinity in coastal waters: A spectrophotometric approach. Mar. Chem. 176: 199–207. doi:10.1016/j.marchem.2015.09.008

Yao, W., and R. H. Byrne. 1998. Simplified seawater alkalinity analysis. Deep-Sea Res. I Oceanogr. Res. Pap. 45: 1383–1392. doi:10.1016/S0967-0637(98)00018-1

Acknowledgments

Conflict of Interest

None declared.